

Radiation Pressure Dominant Acceleration: Polarization and Radiation Reaction Effects in Three Dimensional Particle-In-Cell Simulations

M. Tamburini,^{1,2,*} T. V. Liseykina,³ F. Pegoraro,^{2,1} and A. Macchi^{1,2}

¹*Istituto Nazionale di Ottica, CNR, research unit “A. Gozzini”, Pisa, Italy*

²*Dipartimento di Fisica “E. Fermi”, Università di Pisa, Largo Bruno Pontecorvo 3, I-56127 Pisa, Italy*

³*Institut für Physik, Universität Rostock, D-18051 Rostock, Germany*

(Dated: June 2, 2019)

Polarization and Radiation Reaction (RR) effects in the interaction of a superintense laser pulse ($I > 10^{23} \text{ W cm}^{-2}$) with a thin plasma foil are investigated with three dimensional Particle-In-Cell (PIC) simulations. For a linearly polarized laser pulse, strong anisotropies such as the formation of two high-energy clumps in the plane perpendicular to the propagation direction and significant radiation reaction effects are observed. On the contrary, neither anisotropies nor significant radiation reaction effects are observed for circularly polarized laser pulses. In both cases, the deformation of the initially flat plasma foil leads to the self-formation of a quasi-parabolic shell that focuses the impinging laser pulse up to an energy density more than eight times the initial peak energy density.

PACS numbers: 52.38-Kd, 52.65.Rr

The radiation pressure generated by ultraintense laser pulses may drive strong acceleration of dense matter, as experimentally shown in various regimes [1]. Radiation pressure may thus be an effective mechanism for the generation of high-energy ions, especially in the regime of extremely high intensities and relativistic ion energies as foreseen with the ELI project [2]. In the case of solid-density thin foil targets, Particle-In-Cell (PIC) simulations have shown that at intensities exceeding $10^{23} \text{ W cm}^{-2}$ and for linear polarization (LP) of the laser pulse radiation pressure eventually dominates the acceleration yielding linear scaling with the laser pulse intensity, high efficiency and quasi-monoenergetic features in the ion energy spectrum [3]. Other studies have shown that the use of circular polarization (CP) instead of LP and normal incidence quenches the generation of high-energy electrons [4] allowing radiation pressure to dominate even at lower intensities and leading to efficient acceleration of ultrathin foils [5].

A systematic comparison of LP versus CP in the radiation pressure dominant acceleration (RPDA) regime where ions become relativistic has not been performed yet. To this aim a three-dimensional (3D) approach is important because e.g. in 2D simulations and for LP the laser-plasma coupling is different for *S*- and *P*-polarization (i.e. for the electric field of the laser pulse either perpendicular or parallel to the simulation plane, respectively) and the constraint of the conservation of angular momentum carried by CP pulses holds in 3D only. Multi-dimensional effects in the RPDA regime may play a crucial role as found in 2D simulations which have both shown the onset of instabilities [6] but also a potentially “unlimited” energy gain for the fraction of ions that are phase-locked with the laser-pulse [7]. At the same time, effects such as the tight focusing of the pulse and the transverse bending and expansion of the foil may lead to significant deviation from a plane geometry with a notice-

able heating of electrons even for CP. These effects may eventually spoil the quasi-monoenergetic features of the ion energy spectrum and reduce the fraction of the accelerated ions. Furthermore, it has been shown by 1D PIC simulations that Radiation Reaction (RR) effects may significantly affect the dynamics of radiation pressure acceleration for both thick [8] and thin targets [9, 10], and depend strongly on the laser pulse polarization [9].

In this Letter, we address the role of polarization and RR effects in the RPDA regime using fully 3D PIC simulations where RR effects have been included for the first time in a 3D code. Our results show that also in this regime CP leads to higher ion energies and better collimation than for LP, for which an anisotropic ion distribution is observed. It is also found that the bending of the foil leads to a self-generated parabolic shell that focuses the impinging pulse down to an almost λ^3 scale and that the energy density at the focus exceeds the initial peak energy density by a factor of ~ 5 for LP and ~ 8 for CP. Compared to 2D simulations with analogous parameters, the pulse focusing effect is enhanced and the cut-off energy of ions is increased. RR effects on the ion spectrum are found to be negligible for CP but quite relevant for LP where they increase the energy cut-off.

Our approach is based on the numerical solution of kinetic equations for the phase space distributions of electron and ions, where RR is included in the motion of electrons via the Landau-Lifshitz (LL) force [11]. Details of the RR modeling are given in Refs.[9, 12]. In order to clarify the new qualitative features due to RR effects, we recall that the phase space volume element J evolves according to $dJ/dt = J \nabla_{\mathbf{p}} \cdot \mathbf{f}_R$ where \mathbf{f}_R is the RR force. It has been shown [12] that $\nabla_{\mathbf{p}} \cdot \mathbf{f}_R \leq 0$ and therefore the RR force leads to a *contraction* of the available phase space volume. The physical interpretation of this property is that the RR force acts as a cooling mechanism for the system accounting for the emission of high-energy

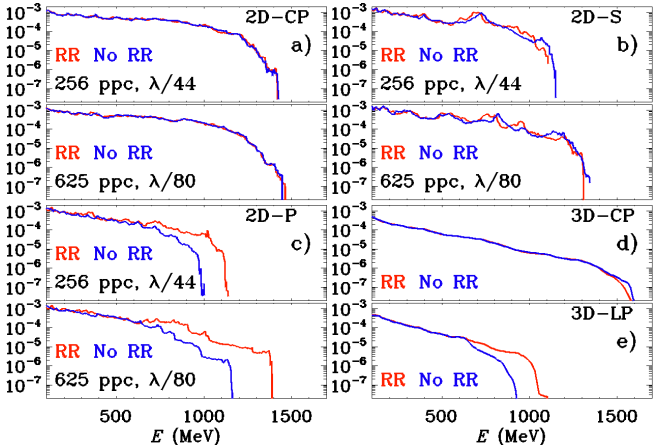


FIG. 1. Ion spectra from 2D [a-c)] and 3D [d-e)] simulations with same physical parameters, all at $t = 20T$. The 2D spectra are reported for circular (CP, frame a)) and linear (LP) “S” (frame b)) and “P” (frame c)) polarization cases. In each plot, the blue and red curves correspond to simulations without and with radiation reaction (RR) effects, respectively. In the upper plots of frames a-c) the numerical resolution (number of particles per cell and of points per wavelength) is similar to those of the 3D simulations in d-e), while in the lower plots the results for higher resolution are shown.

photons. These photons are assumed to escape from the plasma freely, carrying away energy, momentum and entropy [12].

We present a total of four 3D simulations each with the same physical and numerical parameters but different polarization, with and without RR effects. In these simulations, the laser field amplitude has a \sin^2 -function longitudinal profile with 8λ FWHM (where $\lambda = 0.8 \mu\text{m}$ is the laser wavelength) while the transverse radial profile is Gaussian with 10λ FWHM and the laser pulse front reaches the edge of the plasma foil at $t = 0$. The peak intensity at the focus is $I = 1.7 \times 10^{23} \text{ W cm}^{-2}$ which corresponds to a normalized amplitude $a_0 = 280$ for LP and $a_0 = 198$ for CP. The target is a plasma foil of electrons and protons with uniform initial density $n_0 = 64n_c$ (where $n_c = \pi m_e c^2 / e^2 \lambda^2$ is the critical density), thickness $\ell = 1\lambda$ and initially located in the region $10\lambda \leq x \leq 11\lambda$. The simulation grid is $1320 \times 896 \times 896$ and the spatial step is $\lambda/44$ for each direction. The timestep is $T/100$ where $T = \lambda/c = 2.67 \text{ fs}$ is the laser period. We use 216 particles per cell for each species and the total number of particles is 1.526×10^{10} . The runs were performed using 1024 processors of the IBM-SP6 cluster at the CINECA supercomputing facility in Bologna, Italy.

Large-scale 3D PIC simulations are limited by the size and availability of computational resources both in the numerical resolution and in the number of runs that may be performed. These issues may raise doubts on the ac-

curacy of 3D results. To gain confidence on this side, prior to 3D runs we performed 2D simulations both with numerical parameters similar to those of 3D runs and with higher accuracy. The effect of increasing resolution and particle number on the ion spectra in 2D simulations is shown in Fig.1 where 2D results are reported for the three different polarization cases (CP, LP-S and LP-P) and compared with the 3D results for both LP and CP. In the CP case both numerical and RR effects on the spectrum are smaller while in the P -polarization case these effects are larger. Changing the spatial resolution from $\lambda/44$ to $\lambda/80$ and increasing the number of particles-per-cell (ppc) for each species from 256 to 625 shifts the energy cut-off by $\sim 2\%$ in the CP case and by $\sim 15\%$ ($\sim 20\%$) in the P -polarization case without RR. The stronger effect of the inclusion of RR for the higher resolution case may be explained by noticing that RR mostly affects the highest energy electrons, which are located in the tail of the distribution function that needs a very high number of particles to be resolved properly. Nevertheless, the limited resolution does not qualitatively affect prominent features in ion spectra, such as the higher energy for CP and the relevance of RR effects for LP only, leading for this latter case to an *higher* energy of ions as observed in 1D simulations [9]. At the same time, 2D and 3D spectra show new features such as an higher cut-off energy in 3D than in the 2D case, and the fact that P -polarization leads to a much stronger RR effect than the S -polarization case.

Figure (2) shows the ion and the electron 3D spatial distributions at $t = 20T$ for the LP case without (a) and with (b) RR and for the CP case without (c) and with (d) RR. The color corresponds to the range in kinetic energy. In the LP case the most energetic ions are grouped into two off-axis clumps lengthened and aligned along the polarization direction. The second most energetic ion population is also stretched along the polarization direction with two off-axis clumps and a widespread central clump, in which ions are grouped asymmetrically. The density of this latter population is smaller than that of the two higher-energy clumps.

RR effects are much stronger for LP, where the density and the total number of ions grouped into the highest energy populations is strongly enhanced in the case with RR as seen by the comparison of Figs.2 a) and b) and also in Figs.3 a1), a2) and b1), b2) where sections of the ion density in the (x, y) and (x, z) planes are shown. The contours of the electromagnetic (EM) energy density in Figs.3 a1), a2) and b1), b2) show that near the axis most of the laser pulse have been transmitted through the target. The increased bunching and higher density observed in the case with RR may be related to the higher ion energies since the local increase of the density and therefore of the reflectivity leads to a longer and more efficient RPDA phase. This is consistent with observing in Figs.3 b1) and b2) that the EM energy density is higher off-axis

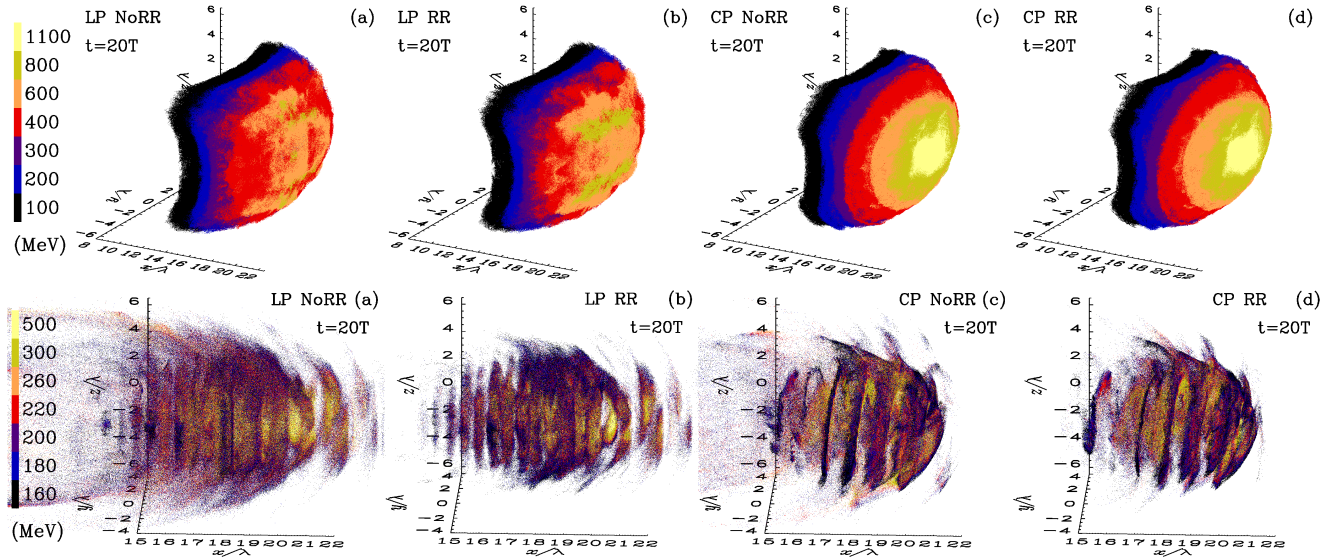


FIG. 2. Spatial distributions of ions (upper row) and electron (lower row) at $t = 20T$ and in the region $-5.7 \leq (y, z)/\lambda \leq 5.7$, for LP without (a) and with (b) RR and for CP without (c) and with (d) RR. Ions and electrons are divided into seven populations according to their kinetic energy, with the color-bar reporting the lower bound of the energy interval. In the LP case (frames (a,b)), the polarization is along the y axis.

and behind the high-density clumps, which correspond to the most energetic ions. The high-energy clumps observed in the LP case are also similar to the ion lobes observed in Ref.[13] at lower intensity but still in a regime of strong pulse penetration through the foil. RR effects play a minor role for CP affecting only a small fraction of ultra-relativistic electrons with almost no influence on the ion distribution as seen in Fig.2, frames c),d). For CP, the ion spatial distribution follows the spatial intensity profile of the initial laser pulse, has rotational symmetry around the central axis, and a distribution in energy monotonically decreasing with increasing radial distance. The most energetic ions ($E \geq 1100$ MeV) are located near the axis. No population in the same energy interval is present in the LP case (compare frames (a,b) with (c,d) in Fig.2). The electron spatial distribution has an helicoidal shape with step λ Fig.2 (c), (d).

The differences between CP and LP can be explained by the absence of the oscillating component of the $\mathbf{J} \times \mathbf{B}$ force for CP [4]. Thus, in the CP case we have a steady push of the foil with weak penetration of the laser pulse in the plasma. Most of the electrons move coherently with the foil and in the same direction as the laser pulse so that the RR force may also becomes very small [3, 9]. For LP pulses, the longitudinal oscillations driven by the 2ω component of the $\mathbf{J} \times \mathbf{B}$ force result into a strong electron dispersion and heating yielding a significant decrease of the electron density and penetration of the pulse. The much stronger RR effects in the LP case are accounted for by both the strongest penetration of the laser pulse

and the $\mathbf{J} \times \mathbf{B}$ -driven oscillations of the electrons causing them to collide with the counterpropagating laser pulse twice per cycle [9]. Our 2D and 3D results confirm the strong differences between CP and LP also for a focused laser pulse and a strongly bent target. At the same time, the 2D and 3D results suggest that the “ P ” component of the electric field \mathbf{E} (not present in 1D geometry) strongly contributes to enhanced electron heating and dispersion, pulse penetration and RR effects. Such component is present both in the LP case and in the 2D case with P -polarization and its importance accounts for the similarity between the corresponding spectra in Fig.1 c) and e). For LP, the laser pulse significantly penetrates into the foil from the beginning of the interaction. After this initial phase, electrons and ions are dispersed laterally and asymmetrically by the y -component of the electric field. This lateral dispersion leads to a further decrease of the electron density and eventually the laser pulse breaks through the foil as seen in Fig.3, frames (a1-d1) and (a2-d2). Electrons thus move into strong fields of the same order of the vacuum fields and clear signs of RR effects appear both in the electron and in the ion distribution. As shown in frames (a,b) of Fig.2, the spatial distribution electrons also show a quasi-periodical distribution with a $\sim \lambda/2$ wavelength.

The 2D sections of the total electromagnetic energy density and of the electron and ion densities in Fig.3 show a self-generated parabolic shell wrapping the laser pulse. In the CP case, a mark of the helicoidal electron distribution is present in the form of strong modulations of

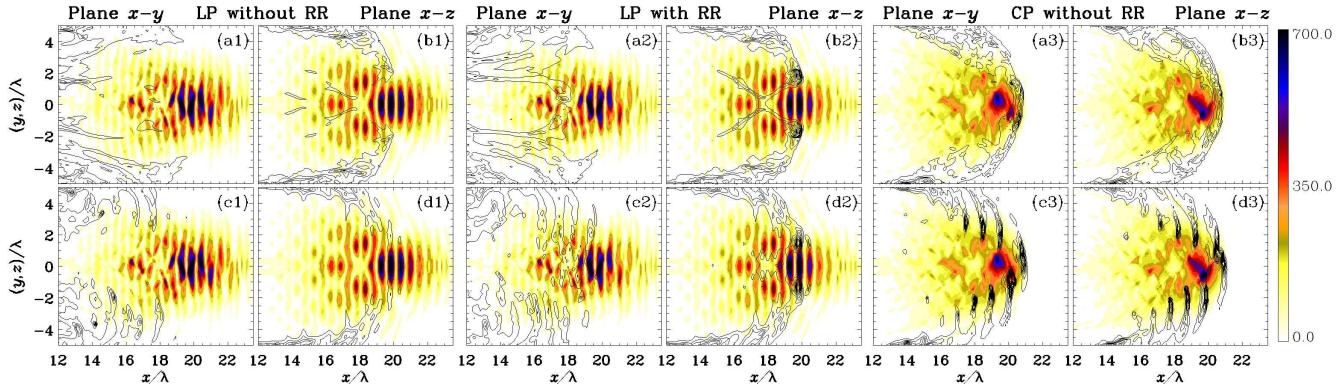


FIG. 3. 2D sections of the laser pulse-foil interaction at $t = 20T$. Each frame reports the color contours of $\sqrt{E^2 + B^2}$ (normalized units) in the $x - y$ plane at $z = 0$ (a1-3 and c1-3) and in the $x - z$ plane at $y = 0$ (b1-3 and d1-3). Black contours of the *ion* density are superimposed for LP without (a1,b1) and with (a2,b2) RR and for CP without RR (a3,b3). Black contours of the *electron* density are superimposed for LP without (c1,d1) and with (c2,d2) RR and for CP without RR (c3,d3). The CP case with RR is almost identical to the CP case without RR and it is not reported.

the shell while in the LP case the two denser and higher-energy clumps are clearly visible in the $x - z$ plane. In the CP case, this self-generated parabola focuses the impinging laser pulse up to nearly a λ^3 scale and both the energy and the momentum densities at the focus reach values more than eight times their peak value in the initial laser pulse. The self-generated parabola is present also in the LP case even though its focusing effect is slightly reduced as the laser pulse breaks through the parabolic shell and both the energy and momentum densities reach values more than five times their peak value in the initial laser pulse. The focusing effect is significantly stronger in 3D where the energy density at the focus is more than tripled (doubled) for linear (circular) polarization compared to the analogous 2D case. This effect may explain the higher peak energy on axis observed in 3D, Fig.1 d) with respect to the 2D case, Fig.1 a).

In conclusion, we studied polarization and radiation reaction effects on ion acceleration in the radiation pressure dominant regime with three-dimensional particle-in-cell simulations. A strong dependence on the laser pulse polarization has been observed, confirming and extending previous results obtained for lower intensity and/or lower dimensionality. For circular polarization the ion spatial distribution follows the spatial intensity distribution of the impinging laser pulse with the most energetic ions on the symmetry axis and almost no radiation reaction effects. In the linear polarization case, lower maximum energies are achieved, the most energetic ions are grouped into two off-axis clumps and radiation reaction effects significantly affect the energy spectrum. In both cases, a self-generated parabola focuses the impinging pulse and the energy density at the focus reaches values nearly one order of magnitude higher than the initial peak values. We expect these findings to be of relevance for the design of future experiments on laser acceleration of ions up to

relativistic (GeV) energy.

Work sponsored by the Italian Ministry of University and Research via the FIRB project “SULDIS”. We acknowledge the CINECA Award N.HP10A25JKT-2010 for the availability of high performance computing resources.

* E-mail: tamburini@df.unipi.it

- [1] S. Kar et al., Phys. Rev. Lett. **100**, 225004 (2008).
K. U. Akli et al., Phys. Rev. Lett. **100**, 165002 (2008).
A. Henig et al., Phys. Rev. Lett. **103**, 245003 (2009).
C. A. J. Palmer et al., Phys. Rev. Lett. **106**, 014801 (2011).
- [2] Note1, <http://www.eli-laser.eu>.
- [3] T. Esirkepov, M. Borghesi, S. V. Bulanov, G. Mourou, and T. Tajima, Phys. Rev. Lett. **92**, 175003 (2004).
- [4] A. Macchi, F. Cattani, T. V. Liseykina, and F. Cornolti, Phys. Rev. Lett. **94**, 165003 (2005).
- [5] X. Zhang, B. Shen, X. Li, Z. Jin, and F. Wang, Phys. Plasmas **14**, 073101 (2007).
A. P. L. Robinson, M. Zepf, S. Kar, R. G. Evans, and C. Bellei, New J. Phys. **10**, 013021 (2008).
O. Klimo, J. Psikal, J. Limpouch, and V. T. Tikhonchuk, Phys. Rev. ST Accel. Beams **11**, 031301 (2008).
- [6] F. Pegoraro and S. V. Bulanov, Phys. Rev. Lett. **99**, 065002 (2007).
- [7] S. V. Bulanov et al., Phys. Rev. Lett. **104**, 135003 (2010).
- [8] N. Naumova et al., Phys. Rev. Lett. **102**, 025002 (2009).
- [9] M. Tamburini, F. Pegoraro, A. Di Piazza, C. H. Keitel, and A. Macchi, New J. Phys. **12**, 123005 (2010).
- [10] M. Chen, A. Pukhov, T.-P. Yu, and Z.-M. Sheng, Plasma Phys. Contr. Fusion **53**, 014004 (2011).
- [11] L. D. Landau and E. M. Lifshitz, *The Classical Theory of Fields* (Elsevier, Oxford, 1975), 2nd ed.
- [12] M. Tamburini et al., Nucl. Inst. Meth. Phys. Res. A (2011), in press, doi: 10.1016/j.nima.2010.12.056.
- [13] L. Yin et al., Phys. Rev. Lett. **107**, 045003 (2011).